# Quantitative analysis of non-equilibrium systems from short-time experimental data

**Sreekanth K Manikandan**
NORDITA, KTH Royal institute of technology and Stockholm university, Stockholm
**Subhrokoli Ghosh**
Indian Institute of Science Education and Research Kolkata
**Avijit Kundu**
Indian Institute of Science Education and Research Kolkata
**Biswajit Das**
Indian Institute of Science Education and Research Kolkata
**Vipin Agrawal**
NORDITA, KTH Royal institute of technology and Stockholm university, Stockholm
**Dhrubaditya Mitra**
NORDITA, KTH Royal institute of technology and Stockholm university, Stockholm
**Ayan Banerjee**
Indian Institute of Science Education and Research Kolkata https://orcid.org/0000-0003-2443-9125
**Supriya Krishnamurthy** ( supriya@fysik.su.se )
Stockholm University

**Article**

**Keywords:** Thermodynamic Uncertainty Relation (TUR), quantitative analysis, colloidal particle system, thermodynamic force

**Posted Date:** March 19th, 2021

**DOI:** https://doi.org/10.21203/rs.3.rs-310152/v1



**Version of Record:** A version of this preprint was published at Communications Physics on December 1st, 2021. See the published version at https://doi.org/10.1038/s42005-021-00766-2.

# Quantitative analysis of non-equilibrium systems from short-time experimental data

Sreekanth K Manikandan[1,4], Subhrokoli Ghosh[2,4], Avijit Kundu[2], Biswajit Das[2], Vipin Agrawal[1,3], Dhrubaditya Mitra[1,3,*] Ayan Banerjee[2,†] and Supriya Krishnamurthy[3‡]
[1]*NORDITA, KTH Royal institute of technology and Stockholm university, Stockholm.*
[2]*Department of Physical Sciences, IISER Kolkata, India*
[3]*Department of Physics, Stockholm University, SE-10691 Stockholm, Sweden and*
[4]*These authors contributed equally: Sreekanth K Manikandan and Subhrokoli Ghosh*
(Dated: March 8, 2021)

We provide a minimal strategy for the quantitative analysis of a large class of non-equilibrium systems in a steady state using the short-time Thermodynamic Uncertainty Relation (TUR). From short-time trajectory data obtained from experiments, we demonstrate how we can simultaneously infer quantitatively, both the thermodynamic force field acting on the system, as well as the exact rate of entropy production. We benchmark this scheme first for an experimental study of a colloidal particle system where exact analytical results are known, before applying it to the case of a colloidal particle in a hydrodynamical flow field, where neither analytical nor numerical results are available. Our scheme hence provides a means, potentially exact for a large class of systems, to get a quantitative estimate of the entropy produced in maintaining a non-equilibrium system in a steady state, directly from experimental data.

Non-Equilibrium thermodynamics at microscopic length scales is dominated by a fascinating range of phenomena [1], where thermal fluctuations play a crucial role. These phenomenon can now be observed in great detail experimentally, due to the availability and scope of current microscopic manipulation techniques. The interpretation and quantitative analysis of the experimentally available data is however lagging behind these advances, mostly due to the fact that the vast majority of these systems are too complicated to model without making several approximations, despite having far fewer degrees of freedom than their macroscopic counterparts. Even when it is possible to build such simplified models, these are still usually too complicated to solve except sometimes by numerical analysis of specific systems, which however lack general insights. There could also be other factors making the system hard to solve, such as the presence of a background flow, for which the spatial dependence of the flow velocity needs to be known by means of solving the corresponding Navier-Stokes equation; usually a difficult task, especially for unsteady flows. In the face of all these challenges, a relevant question is whether it is at all possible to gain any precise quantitative information about a complex non-equilibrium system directly from experimental data, bypassing the first step of either having a known model to compare with or building in simplifying assumptions about the system.

Not surprisingly, this question has aroused a lot of recent interest. Broadly speaking, measurements from experiments can be used to obtain general information about the system, such as identifying that detailed balance is broken and hence the system is out-of-equilibrium [2–4] (not always obvious for microscopic systems such as at the cellular level), or to obtain more specific properties of the system such as the rate of dissipation of energy (equivalently the rate of entropy production) [5–12], the average phase-space velocity field [2, 13, 14] related to the so-called thermodynamic force field [15, 16] or the microscopic forces driving the system [14, 17]. The motivation for such studies is that if quantitative information about the system can be directly obtained from experimentally observed quantities, then this understanding can be used for building more realistic and experimentally validated models of the system of interest [2, 18, 19].

A very informative quantity about a non-equilibrium system is the rate of entropy production. This quantity not only signals - when it is non-zero - that the system is out of equilibrium, but also provides a quantitative measure of how out-of-equilibrium a system is and the irreversibility of the dynamics [20–22]. In the context of microscopic machines [23], a quantification of the amount of energy dissipated directly provides information about engine efficiencies [24–26] and prescriptions for obtaining optimal operating conditions [27]. The value of the entropy production rate can also be used to obtain information-theoretic quantities of interest [28], or even information about hidden degrees of freedom [29].

The entropy production rate can be obtained directly from experimental data, at least for systems where it is understood that the underlying dynamics is Markovian, by several means. These include utilizing the Harada-Sasa equality [5] which involves a spectral analysis of trajectory data [30, 31], determining the average steady state current and steady-state probability distribution from the data [6], determining the time-irreversibility of the dynamics [22, 32–36] and relatedly determining esti-

* dhruba.mitra@gmail.com
† ayan@iiserkol.ac.in
‡ supriya@fysik.su.se

mators for the ratio of forward and backward processes directly from the data [9, 37, 38]. Very recent approaches [11, 14] also advocate inferring first the microscopic force field from which the entropy production rate can be inferred.

An alternative strategy is to set lower bounds on the entropy production rate [39–43] by measuring experimentally accessible quantities. One class of these bounds, for example those based on the thermodynamic uncertainty relation (TUR) [43–47], have been further developed into variational *inference* schemes which translate the task of identifying entropy production to an optimization problem over the space of a single projected fluctuating current in the system [10, 48–50]. Recently, a similar variational scheme using neural networks was also proposed [51]. As compared to other trajectory-based entropy estimation methods, these inference schemes do not involve the estimation of probability distributions over the phase-space, rather they usually only involve means and variances of measured currents, and are hence known to work better in higher dimensional systems [10]. In addition, it is proven that such an optimization problem gives the exact value of the entropy production rate in a stationary state as well as the exact value of the thermodynamic force field, if short-time currents are used [48–51]. However, these methods have not yet been tested against experimental data to the best of our knowledge.

Here we demonstrate that the Short-time TUR based inference scheme can be used to infer both the entropy production as well as the thermodynamic force field in different experimental setups involving colloidal particles in (time-varying) potentials. We first test the scheme in an experimental set up where the entropy production rate of the system can also be analytically predicted, hence benchmarking our procedure. We then apply the scheme to a modified system for which the underlying model is both unknown and hard to estimate. The short-time TUR predicts a value of the entropy prediction even for this situation. We provide a motivation for the value as well as demonstrate how we might infer some useful properties of this system by knowing the value of the entropy production rate of the system.

## MODEL

The results we demonstrate here apply to systems with continuous state-space but a finite-number of degrees of freedom, described by overdamped Langevin equations of the type

$$\dot{X}_\mu(t) = F_\mu[\boldsymbol{X}(t)] + G_{\mu\nu}[\boldsymbol{X}(t)] \cdot \xi_\nu, \tag{1}$$

Here $\mu = 1, \ldots, N$ is the number of degrees of freedom of the system and we use $\cdot$ to refer to the Ito convention. $F_\mu(\boldsymbol{X})$ is a function of $\boldsymbol{X}$, but not an explicit function of time,t, $\xi_\mu$ is $N$ dimensional white-in-time noise such that $\langle \xi_\mu(t)\xi_\nu(t')\rangle = \delta_{\mu\nu}\delta(t-t')$, where $\langle\cdot\rangle$ denotes averaging over the statistics of the noise. The corresponding Fokker–Planck equation for the probability distribution function $P$ is given by:

$$\partial_t P = -\partial_\mu J_\mu \quad , \tag{2a}$$

$$J_\mu \equiv F_\mu P - D_{\mu\nu}\partial_\nu P, \qquad D_{\mu\nu} = \frac{1}{2} G_{\mu\alpha} G_{\alpha\nu}. \tag{2b}$$

In the stationary state $\partial_t P = 0$. The total rate of entropy production $\sigma$ can be obtained as [6, 34],

$$\sigma = \int d\boldsymbol{X}\ \mathcal{F}_\mu J_\mu \quad \text{where} \tag{3a}$$

$$\mathcal{F}_\mu \equiv \frac{D^{-1}_{\mu\nu} J_\nu}{P} \tag{3b}$$

is called the thermodynamic force field [10]. Overdamped Langevin equations are excellent descriptions for colloidal particle systems. Even for systems where the Langevin equation is not known, the fact that such a description exists in principle is all that is needed in order to apply Eq. 3a and obtain $\sigma$ by determining the current and steady-state probability density directly from the time-series data [6, 10]. Another approach is to first infer the terms in the Langvein equation, $F_\mu$ and $D$ [11, 14] and use Eq. 3a to obtain $\sigma$. These methods can be applied directly on data obtained from tracking the system or by even using tracking-free methods in image space [11]. Note however that all these methods require the measurement or empirical estimation of the steady-state probability distribution $P$, its spatial derivatives and current $J_\mu$.

## RESULTS

In this paper, we demonstrate an alternative method for the simultaneous determination of both the entropy production rate as well as the thermodynamic force field $\mathcal{F}_\mu$ from experimental data, using the recently introduced short-time thermodynamic inference relation [48–50]. Our method is built on an exact result obtained in [48–50]:

$$\sigma = \max_J \left[ \frac{2k_{\mathrm{B}} \langle J \rangle^2}{\Delta t \mathrm{Var}(J)} \right], \tag{4}$$

where $k_{\mathrm{B}}$ is the Boltzmann constant and $J$ is a scalar current in the non-equilibrium stationary state. This holds for any $\boldsymbol{X}$ that is even under time reversal [52]. Let us now discretize $\boldsymbol{X}$ in time with time interval $\Delta t$: $X^0_\mu \cdots X^{\mathrm{j}}_\mu \cdots X^{\mathrm{N}}_\mu$. We use latin indices as superscripts for the discrete time labels. For a given function $\boldsymbol{d}(\boldsymbol{X})$ we can define a time-discretised scalar current

$$J^{\mathrm{k}} = d_\mu \left( \frac{\boldsymbol{X}^{\mathrm{k}} + \boldsymbol{X}^{\mathrm{k+1}}}{2} \right) \left( X^{\mathrm{k+1}}_\mu - X^{\mathrm{k}}_\mu \right) \tag{5}$$

Any such current can be shown to give a lower bound to $\sigma$. Our algorithm is as follows:

1. We first obtain a time-series of experimental data: $\boldsymbol{X}^{\mathrm{k}}$.

2. To be able to perform maximisation we use a basis in the space spanned by $\boldsymbol{X}$ with basis functions $\psi_m(\boldsymbol{X})$, $m = 1, \ldots, M$, such that

$$\boldsymbol{d}(\boldsymbol{X}) = \sum_{m=1}^{M} \boldsymbol{w}_m \psi_m(\boldsymbol{X}). \tag{6}$$

3. We start with an initial guess for $w_m$, calculate the time-series $J^k$, construct the function within the square brackets in (4) and then maximise over $w_m$ to obtain $\sigma$ and also the set of values $w_m^*$ such that $d^* = \sum_{m=1}^{M} w_m^* \psi_m(\boldsymbol{X})$ maximises Eq. (4).

Furthermore, it is shown in [48] that the thermodynamic force is given by the $\boldsymbol{d}$ that maximises (4), i.e.,

$$\mathcal{F} \propto d^* \tag{7}$$

Hence, by solving an optimization problem, where the RHS of Eq. (4) is maximized in the space of all currents we can obtain $\sigma$ as the optimal value as well as its conjugate thermodynamic force field, $\mathcal{F}_\mu$ up to a constant multiplier. This constant multiplier can in addition, be fixed by using $\mathrm{Var}(\Delta S_{tot}) = 2\langle \Delta S_{tot} \rangle$ at $\tau \to 0$ [48].

We note that similar algorithms have already been tested against numerical data generated from steady-state colloidal particle systems [49, 50] in the context of the short-time inference scheme. Here we test this scheme in an experimental setup.

*Colloidal particle in a stochastically shaken trap*

To test the inference scheme we first apply it to an experimental problem for which the rate of entropy production is known from theory [53–56] – a colloidal particle in a stochastically shaken optical trap. This model was first experimentally tested in [57].

We trap a polystyrene particle in an optical trap; see the methods section for details of how the experiment is performed. We modulate the position of the center of the trap $\lambda(t)$ along a fixed direction $x$ on the trapping plane perpendicular to the beam propagation ($+z$). The modulation is a Gaussian Ornstein-Uhlenbeck noise with zero mean and covariance $\langle \lambda(0)\lambda(s) \rangle = A \exp(- \mid s \mid /\tau_0)$, i.e.,

$$\dot{\lambda}(t) = -\frac{\lambda(t)}{\tau_0} + \sqrt{2A}\eta, \tag{8}$$

where $\eta$ is Gaussian, has zero-mean and is white-in-time. The correlation time $\tau_0$ is held fixed for all our experiments.

The dynamics of the colloidal particle is well described by an overdamped Langevin equation,

$$\dot{x}(t) = -\frac{K}{\gamma}\left[x(t) - \lambda(t)\right] + \sqrt{2D}\xi, \tag{9}$$

where $K$ is the spring constant of the harmonic trap, $\gamma$ is the drag coefficient, $\xi$ is the thermal noise, $D = k_{\mathrm{B}}T/\gamma$ is the diffusion coefficient of the particle and $T$ the temperature of the medium. The noise $\xi$ is also Gaussian, zero-mean and white-in-time and mutually independent from the noise $\eta$ in Eq. 8. Note that $A\tau_0$ can be interpreted as an effective temperature [58]. Equations (9) and (8) together define the model we call the Stochastic Sliding parabola. Starting from arbitrary initial conditions for $x$ and $\lambda$, the system reaches a non-equilibrium stationary state, with the probability distribution function and current given respectively by [59]

$$P(x,\lambda) = \frac{\exp\left(-\frac{(\delta+1)\left(\delta^2\theta(x-\lambda)^2+\delta\left(\theta x^2+\lambda^2\right)+\lambda^2\right)}{2D\tau_0\theta\left(\delta^2(\theta+1)+2\delta+1\right)}\right)}{2\pi\sqrt{\frac{D^2\tau_0^2\theta\left(\delta^2(\theta+1)+2\delta+1\right)}{\delta(\delta+1)^2}}}, \tag{10a}$$

$$J(x,\lambda) = \begin{pmatrix} \frac{\delta\left(\delta^2\theta(\lambda-x)+\delta\lambda+\lambda\right)}{\left(\delta^2(\theta+1)+2\delta+1\right)\tau_0} \\ -\frac{\delta^2\theta(\delta x+x-\delta\lambda)}{\left(\delta^2(\theta+1)+2\delta+1\right)\tau_0} \end{pmatrix} P(x,\lambda), \tag{10b}$$

where the dimensionless parameters $\theta$ and $\delta$ are defined as,

$$\delta = \frac{K\tau_0}{\gamma}, \qquad\qquad \theta = \frac{A}{D}. \tag{11}$$

The rate of entropy production and the thermodynamic force field for this model are,

$$\sigma = \frac{\delta^2\theta}{(\delta+1)\tau_0}, \tag{12a}$$

$$\boldsymbol{\mathcal{F}}(\boldsymbol{x}) \equiv \begin{pmatrix} \mathcal{F}_x \\ \mathcal{F}_y \end{pmatrix} = \begin{pmatrix} \frac{\delta\left(\delta^2\theta(\lambda-x)+\delta\lambda+\lambda\right)}{D\tau_0\left(\delta^2(\theta+1)+2\delta+1\right)} \\ -\frac{\delta^2(\delta x+x-\delta\lambda)}{D\tau_0\left(\delta^2(\theta+1)+2\delta+1\right)} \end{pmatrix} \tag{12b}$$

In Fig. 1 we compare the above exact results to the outcome of the inference algorithm applied to numerically generated data for this model. Different sets of time-series data were generated by varying the noise amplitude ratio $\theta$, keeping the other parameters fixed. In Fig. 1a, we see that the inference algorithm predicts an estimate of $\sigma$ very close to the true value. The inference algorithm also simultaneously gives an optimal force field $\boldsymbol{d}^*(x)$ which is very similar to the thermodynamic Force field $\boldsymbol{\mathcal{F}_\mu(x)}$ expected from theory. We illustrate this in Fig. 1b. From Eq. (12), it is clear that $\sigma$ increases linearly with $\theta$ or equivalently the parameter $A$. Fig 1c illustrates that the inference algorithm captures this behaviour accurately. Since we are limited by the minimal resolution of the time series in probing the $\Delta t \to 0$ limit of Eq. (4), the inferred value of entropy production

is in general different from the exact value by an $\mathcal{O}[\Delta t]$ term. For this model we can also compute this correction analytically as (using expressions previously obtained in [56]),

$$\sigma_{\Delta t} = \sigma - \frac{\delta^4\theta^2\left(\delta^2(\theta+1)+1\right)}{(\delta+1)^2\tau_0^2\left(\delta^2(\theta+1)+2\delta+1\right)}\Delta t + \mathcal{O}[\Delta t]^2, \tag{13}$$

where $\sigma_{\Delta t}$ is the result one gets from Eq. (4) for a fixed value of $\Delta t$. Notice that the $\mathcal{O}[\Delta t]$ correction increases with the value of $\theta$. We indeed observe this trend in Figure 1c.

Next, we tested the algorithm on experimentally generated data for the same model. In the experiments, we varied $A$ from 0.1 to 0.35 ($\left(\times 0.6\times 10^{-6}\right)^2\ m^2 s^{-1}$), while keeping the other system parameters fixed. Experiments for individual parameter sets were carried out for a duration of 100s, with a sampling rate of 10 KHz for the particle position. Each of these 100s long data sets were further divided into 12.5s long patches, upon which the inference algorithm was then tested. In Fig. 2, we demonstrate the results of the analysis of the experimental data. The blue line and the shaded light-blue region correspond to the theoretically predicted value of the entropy production rate, and the error bounds correspond to the fluctuations in trap stiffness in different experiments (See methods section). We find that the inference scheme works well and gives an excellent estimate of $\sigma$ just as for the numerically generated data, for inference at $\Delta t = 0.1ms$ and $\Delta t = 0.2ms$. Notice that inference at 0.2 ms predicts a lower estimate of $\sigma$ consistent with the fact that the true value is obtained in the $\tau \to 0$ limit according to Eq. (4). Out of all the experiments we performed, roughly 2/3 of the data gave correct estimates for $\sigma$.

As compared to the numerically generated data (see the methods section) however, we did not obtain a perfect agreement between the optimal current $\mathbf{d}^*(\mathbf{x})$ and the thermodynamic force field $\mathcal{F}(\mathbf{x})$ in general, as shown in Fig. 3 where streamline plots are used to show the vector-fields. However we observe that the agreement is better for $A = 0.3$ compared to $A = 0.1$ case. We conclude that, this method might not be efficient in reconstructing the force field from experimental trajectories when the forces are weak in which case experimental noises and algorithmic biases can dominate [60, 61].

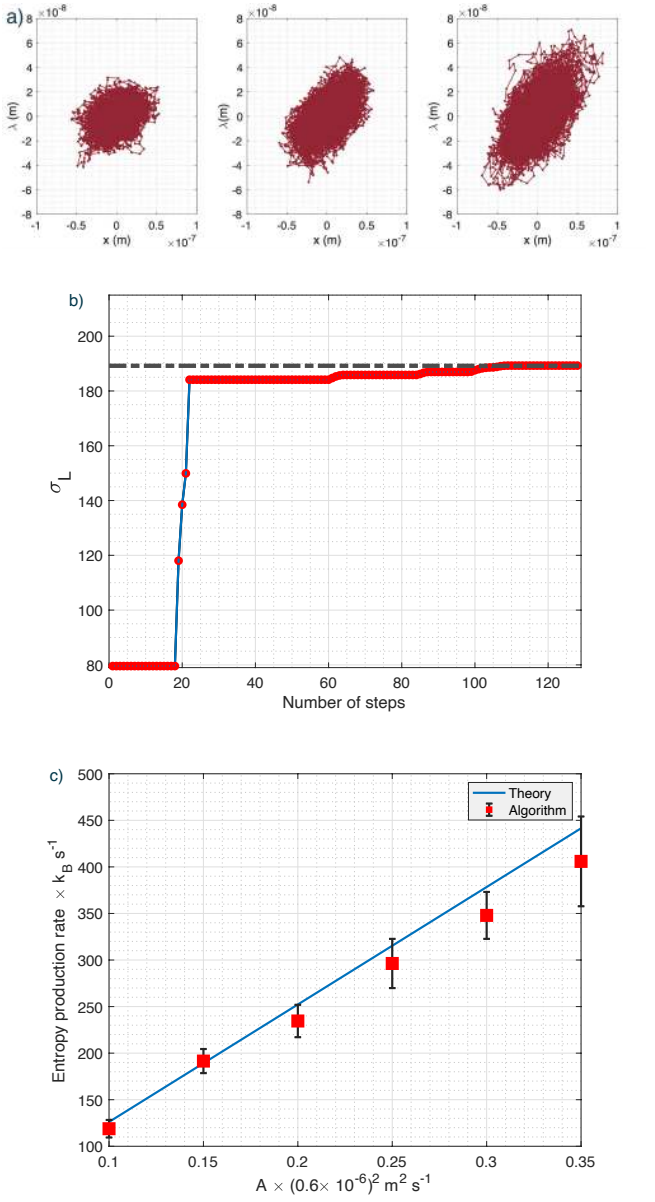


FIG. 1. The inference algorithm tested on numerically generated data. *a)* Brownian trajectories of the *Stochastic sliding parabola* for $A = 0.1$, 0.25 and 0.35. *b)* The inferred entropy production rate plotted against the number of steps in the optimization process for $A = 0.15$ with $\Delta t = 0.0001$. *c)* Inferred entropy production as a function of the parameter $A$.

*A colloidal particle trapped near a microbubble*

After benchmarking our scheme against numerical and experimental data of an analytically solvable system, we apply it to a modified set up where the particle is trapped in the vicinity of a microscopic bubble of size 20-22 $\mu m$. The presence of the bubble sets up flows in its vicinity which affect the trapped colloidal particle and change the steady-state probability distribution. We expect that the underlying description of the particle is still an overdamped Langevin equation, including a flow velocity field $u(x)$. However, the quantification of this flow field is rather difficult, even numerically. As a result, we have a system where the details of the microscopic description are unknown. Our inference scheme, on the other hand, is easily applicable even in this context. In order to demonstrate this, we trap the colloidal particle at different distances from the bubble in a stochastically driven

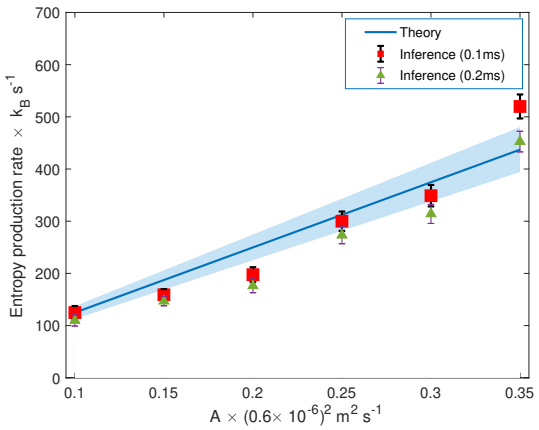


FIG. 2. Inference algorithm tested on the experimental data for different values of the parameter $A$. The blue line corresponds to the theoretical value, and the squares corresponds to $\sigma$ estimated from the experimental data. The shaded blue region accounts for $f_c$ fluctuations theoretically (see the supplemental information).

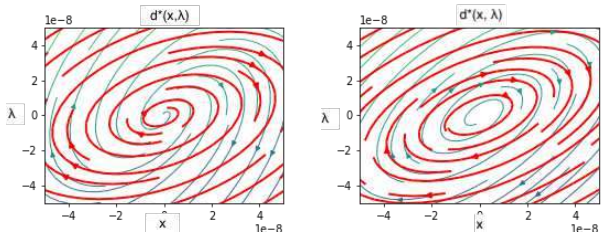


FIG. 3. Optimal force fields (streamline plots) obtained from the experimental data $\mathbf{d}^*(x,\lambda)$ (red) compared to theory $\boldsymbol{\mathcal{F}}(x,\lambda)$ (green) in two cases. The parameter choices used are $A = 0.1$ (*Left*) and $A = 0.3$ (*Right*).

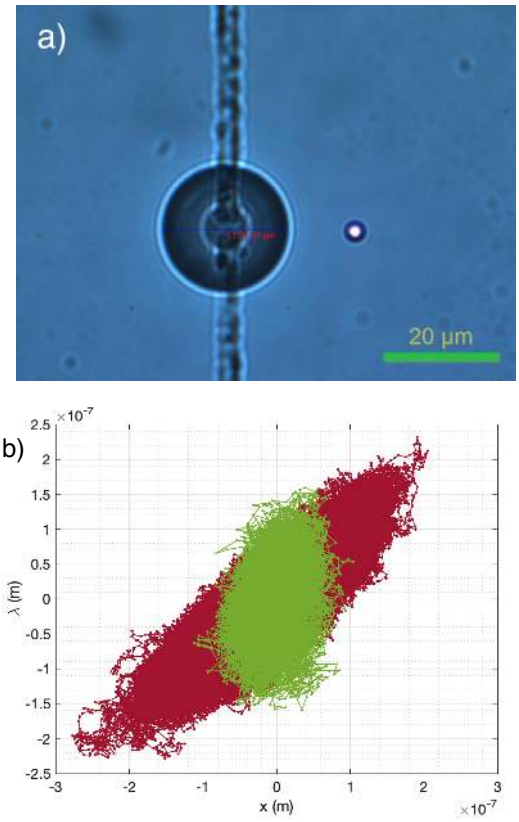


FIG. 4. The colloidal system in the presence of the bubble. a) The microbubble - colloidal particle system. b) System trajectories without (red) and with (green) the bubble in the neighbourhood of the colloidal particle. We see that the colloidal particle is strongly confined in the presence of the bubble.

trap as before, and analyse the experimentally obtained time series data.

At the level of the non-equilibrium trajectories of the system, we see that there is a qualitative difference from the case without the bubble. First, we see that the particle is more confined in the trap when there is a bubble in the vicinity. Further statistical analysis also reveal weaker non-equilibrium currents (see supplemental material, Fig. 9). Consistent with these observations, on applying the inference algorithm, we observe that the value of $\sigma$ is substantially reduced in the presence of the bubble. This is demonstrated in Fig. 4. As we go a distance $d \sim 1.5r$ from the surface of the bubble, we see that the inferred value of $\sigma$ gets closer to the value the system would have had in the absence of the bubble. This is demonstrated in Fig. 5

An important point to understand here, in the light of these findings - is the significance of the inferred value of $\sigma$. In the case without the bubble, it is exactly the total heat dissipated to the environment as a consequence of maintaining the system in a non-equilibrium steady state (by shaking the trap). In the case with the bubble however this is not the case. We present a possible mathematical description of this situation as an overdamped Langevin equation with space-dependent diffusion and damping terms in an unknown flow field $u(x)$. Since the trap constrains the particle motion on scales which are at least two orders of magnitude smaller than the distance to the bubble, $u(x)$ is further assumed to be a constant $u_d$ at a distance $d$ from the surface of the bubble. $\sigma$ calculated from this model, reproduces the values we find from the experimental data, independent of $u_d$, and purely as a consequence of the space-dependent diffusion and damping term, and the two fitting parameters $a$ and $b$. As we discuss in the supplemental material however, there is another component of the entropy production, related to the work that the flow does against the confining potential [37, 62]. This component, which does indeed depend on the value of $u_d$, is not estimated by our inference scheme, due to the fact that $u_d$ is a field (corresponding to the velocities of the molecules of the thermal bath) which is odd under time reversal, for which the TUR does not hold [46, 52, 63–65]. Hence we expect

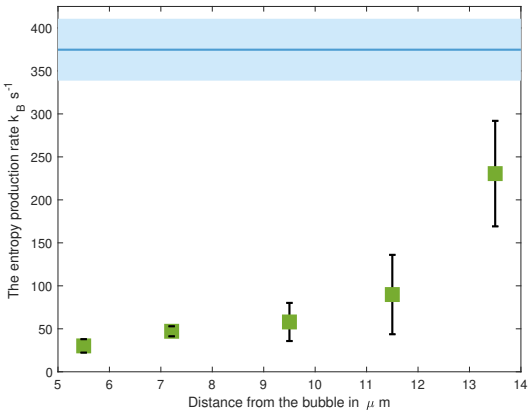


FIG. 5. TUR estimate of entropy production in the colloidal system in the presence of the bubble, as a function of the distance from the surface of the bubble.

that the values of $\sigma$ we find close to the bubble are underestimates of the true value. We elaborate on this point in the supplemental material.

*Mathematical model:* The colloidal system in the presence of the bubble and consequently the flow $u_d$, can be simulated using the following equations:

$$\dot{x} - u_d = -\frac{(x-\lambda)}{\tau_d} + \sqrt{2D_d}\,\eta(t), \tag{14}$$

$$\dot{\lambda} = -\frac{\lambda}{\tau_0} + \sqrt{2A}\,\xi(t), \tag{15}$$

where,

$$\tau_d = \tau\left(a\exp(-bd)+1\right), \tag{16}$$

$$D_d = \frac{D}{a\exp(-bd)+1}. \tag{17}$$

Here the parameters $a$ and $b$ can be tuned to match the experimental data. Particularly, $1/b$ stands for a characteristic length scale over which the flows created by the bubble are significant. When the distance of the trapped particle from the bubble is much greater than $1/b$, the expressions will match the case without the bubble.

In conclusion, we have experimentally tested a simple and effective method, based on the Thermodynamic Uncertainty Relation for inferring the rate of entropy production $\sigma$ and the corresponding thermodynamic force field, in microscopic systems in non-equilibrium steady states [48–50]. We have illustrated the effectiveness of our method for a stochastically driven colloidal system under different non-equilibrium conditions. We expect that this scheme is easily generalizable to a larger number of degrees of freedom and higher dimensions.

It would be very interesting to apply it to other non-equilibrium systems, particularly those, such as molecular motors or certain cellular processes, where our method can give a potentially exact estimate of the dissipation in the system. Recently, Ref. [66] tried to quantify the activity of a cell by measuring the power spectral density of the fluctuations of position of a phagocytosed micron-sized bead *inside a cell*. As it is possible to also trap such beads inside a cell with optical tweezers [66], our technique is ideally suited to be applied to such problems. Finally, in other recent work [67], it has been demonstrated that inference schemes of this kind can also be made to work for non-stationary non-equilibrium states, further diversifying the scope of this class of techniques.

## ACKNOWLEDGEMENT

DM and VA acknowledge the support of the Swedish Research Council through grants 638-2013-9243 and 2016-05225. SK and SKM thank Shun Otsubo for helpful discussions. SKM thanks Ralf Eichhorn for pointing out a useful reference.

## AUTHOR CONTRIBUTION STATEMENT

SK, SKM, AB, DM and SG designed research; SG, AK and BD performed the experiments in AB's lab; VA, SKM and DM implemented the algorithm; VA, SKM and SG analyzed the data; all the authors discussed the results; SKM, SG, SK, DM and AB together wrote the manuscript. SKM and SG contributed equally to the work.

## CODE AVAILABILITY

The Algorithm used to produce the results in this paper is available at: https://doi.org/10.6084/m9.figshare.14174369

## DATA AVAILABILITY

The data used to produce the results in this paper is available at: https://doi.org/10.6084/m9.figshare.14176664

## COMPETING INTERESTS

Authors declare no competing interests.

## Materials and methods

### Experiment

*A single colloidal particle in a stochastically shaken trap*

The experimental setup consists of a sample chamber placed on a motorized xyz-scanning microscope stage, which contains an aqueous dispersion of spherical polystyrene particles (Sigma-Aldrich) of radius $r = 1.5\ \mu m$. The sample chamber consists of two standard glass cover-slips (of refractive index $\sim 1.52$) on top of one another. The thickness of the chamber is kept $\sim 100\ \mu m$ by applying double-sided sticky tape in between the cover-slips. The aqueous immersion is made out of double distilled water at room temperature, which acts as a thermal bath. A single polystyrene particle is confined by an optical trap, which is created by tightly focusing a Gaussian laser beam of wavelength 1064 $nm$ by means of a high-numerical-aperture oil-immersion objective (100x, NA = 1.3) in a standard inverted microscope (Olympus IX71). The trap is kept fixed at a height, $h = 12\ \mu m$ from the lower surface of the chamber in order to avoid spatial variation in the viscous drag due to the presence of the wall. The corner frequency of the trap is set to be $135Hz$. For the first set of experiments, the center of the trap is modulated ($\lambda(t)$) using an acousto-optic deflector, along a fixed direction $x$ in the trapping plane, perpendicular to the beam propagation ($+z$). Thus, the modulation may be represented as a Gaussian Ornstein-Uhlenbeck noise with zero mean and covariance $\langle\lambda(s)\lambda(t)\rangle = A\exp(|t-s|/\tau_0)$. The correlation time $\tau_0$ is held fixed for all our experiments. We determine the barycenter $(x, y)$ displacement of the trapped particle by recording its back-scattered intensity from a detection laser (wavelength 785 nm, co-propagated with the trapping beam) in the back-focal plane interferometry configuration. The measurement is carried out using a balanced-detection system comprising of high-speed photo-diodes [68], with sampling rate of 10 kHz and final spatial resolution of 10 nm.

In the second set of experiments, i.e. for those with the microbubble, we employ a cover slip that is pre-coated by a polyoxometalate material [69, 70] absorbing at 1064 nm as one of the surfaces of the sample chamber (typically bottom surface), and proceed to focus a second 1064 nm laser on the absorbing region. A microbubble is thus nucleated - the size of which is controlled by the power of the 1064 nm laser [69]. Typically we employ bubbles of size between 20-22 $\mu$m. Note that the sample chamber also contains the aqueous immersion of polystyrene particles. We trap a polystyrene probe particle at different distances from the bubble surface, and modulate the trap centre in a manner similar to the experiments without the bubble. The particle is trapped at a axial height corresponding to the bubble radius. The other experimental procedures remain identical to the first set of experiments. An important point here though, is the determination of the distance of the particle from the bubble surface. This we accomplish by using the pixels-to-distance calibration provided in the image acquisition software for the camera attached to the microscope, which we verify by measuring the diameters of the polystyrene particles in the dispersion (the standard deviation of which is around 3% as specified by the manufacturer), and achieve very good consistency. Note that we obtain a 2-d cross-section of the bubble as is demonstrated in Fig. 4, and are thus able to determine the surface-surface separation between the bubble and the particle with accuracy of around 5%. During the experiment, we also ensure that the bubble diameter remains constant by adjusting the power of the nucleating laser - indeed the bubble diameter is seen to remain almost constant for the 100 s that we need to collect data for one run of the experiment.

### Numerical algorithm

Our aim is to maximise a cost function $\mathcal{C}$ which is a function of a set of parameters $\boldsymbol{w}$. We use a particle swarm optimization algorithm [60]. We choose a domain and initialise $N_\mathrm{p}$ particles in that domain. The $k$-th particle follows Newtonian dynamics given by:

$$\frac{d}{dt}\boldsymbol{\omega}^\mathrm{k} = \boldsymbol{V}^\mathrm{k} \tag{18a}$$

$$\frac{d}{dt}\boldsymbol{V}^\mathrm{k} = \boldsymbol{A}^\mathrm{k}(\boldsymbol{\omega}). \tag{18b}$$

Here $\boldsymbol{\omega}^\mathrm{k}$ and $\boldsymbol{V}^\mathrm{k}$ are the position and velocity vector of the $k$-th particle and $\boldsymbol{A}^\mathrm{k}$ is a stochastic function that depends on the position of *all the particles*. Different variants of this algorithm use different $\boldsymbol{A}$. The simplest – the one that we use – is called the *Original PSO*. Let us first define the following:

- The $k$-th particle carries an additional vector $\boldsymbol{P}^\mathrm{k}$ which is equal to $\boldsymbol{\omega}^\mathrm{k}$ for which the value of the function $\mathcal{C}$ as observed by the $k$-th particle was maximum in its history.
- At any point of time let $\boldsymbol{G}$ denote the position of the particle in the whole swarm for which the function has the maximum value.

The function $\boldsymbol{A}$ is given by

$$A^\mathrm{k}_\mu = W_1\delta_{\mu\nu}U^1_\nu(P^\mathrm{k}_\nu - \omega^\mathrm{k}_\nu) + W_2\delta_{\mu\nu}U^2_\nu(G_\nu - \omega^\mathrm{k}_\nu) \tag{19}$$

Here the Greek indices run over the dimension of space. $W_1$ and $W_2$ are two weights. The two terms in Eq. (19) push the particle in two different directions: one towards

the point in history where the particle found the function to be a maxima and the other towards the point where the swarm finds the maximum value of the function at this point of time. These are multiplied by two random vectors $U^1$ and $U^2$ of dimension same as the dimension of space. Each of the components are independent, uniformly distributed (between zero and unity), random numbers.

We keep track of the highest value of the function seen by the swarm and also the location of that point. There are two major advantages to this over standard gradient ascent algorithms: one, it does not require evaluation of the gradient of the function and two, it can be parallellized straightforwardly. All the numerical results reported in this paper are obtained using this algorithm.

### Implementation of the algorithm

Here we describe how we applied the algorithm to numerical/ experimental data. We generate numerical data using first order Euler integration of Eq. (8) and Eq. (9) with a time step of $\Delta t = 0.0001$. In either case we generate many copies of trajectories of length 12.5s, and construct the cost function in Eq. (4) using Eq. (5) and Eq. (6). We have tried out two different choices of basis functions to construct $\boldsymbol{d}(\boldsymbol{X})$. The first one is a Gaussian basis in which we represent $\boldsymbol{d}(\boldsymbol{X})$ as,

$$\boldsymbol{d}(\boldsymbol{X}) = \sum_{m=1}^{M} \boldsymbol{\omega}_m e^{-\frac{(x-x_m)^2}{2b_x^2}} e^{-\frac{(\lambda-\lambda_m)^2}{2b_\lambda^2}}. \qquad (20)$$

Making use of the spatial symmetry of the problem, we assume $\boldsymbol{d}(\boldsymbol{X})$ to be an anti-symmetric function, with $\boldsymbol{d}(-\boldsymbol{X}) = -\boldsymbol{d}(\boldsymbol{X})$, and that reduces the dimensionality of the problem by a factor of 2. Here $M$ is the number of Gaussian functions, and $b_i$ are the variance of the Gaussian in the $x$ and $\lambda$ direction. The centers of the Gaussian $(x_m, \lambda_m)$ are put equally spaced in a rectangular region enclosing the data. Both $M$ and $b_i$ are hyper parameters, and we found that they had negligible effect on the inference. We used $M = 16$ and $b^2_{x/\lambda} = \{x/\lambda\}_{max}/30$. Secondly, we have also tried a linear basis (motivated by the prior knowledge of the linearity of the system) where we take

$$\boldsymbol{d}(\boldsymbol{X}) = \boldsymbol{\omega}_1 x + \boldsymbol{\omega}_2 \lambda. \qquad (21)$$

The particle swarm algorithm we use to find the maximum of the cost function in Eq. (4) in the space of weights $\boldsymbol{\omega}$ is made available here :

Since we have used a finite amount of data to construct the cost function, it will be prone to statistical errors. Therefore we independently maximise the cost function for different 12.5s long data sets, and take their mean value as the optimized estimate of $\sigma$. We show the value of sigma inferred ($\sigma_L$) as a function of the number of steps in the optimization algorithm for different 12.5s long data sets in Fig. 6.

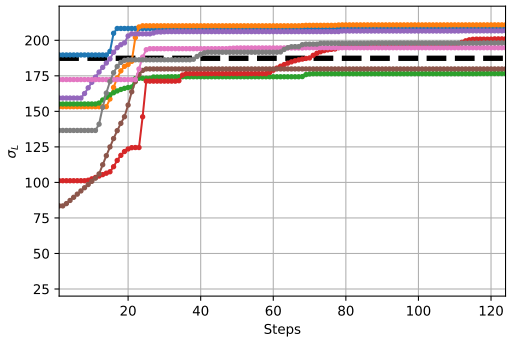


FIG. 6. The value of sigma inferred ($\sigma_L$) as a function of the number of steps in the optimization algorithm for different 12.5s data sets, that are numerically generated for the same parameter choice as in Figure 1b of the main text. The black dashed-line corresponds to the theoretical estimate of $\sigma$ for this parameter choice.

With the numerical data, we also find that the optimal field $d^*$ (see Eq. (6)) is proportional to the thermodynamic fore field $\mathcal{F}$ (Eq. (7)). We demostrate this in Fig. 7.

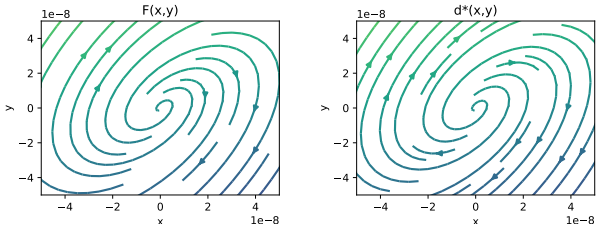


FIG. 7. *Left:* The thermodynamic force field (*streamline plots*) from theory for the same parameter choice as in Figure 1b of the main text. *Right:* The optimal $d^* \propto \mathcal{F}$ obtained from the algorithm for the same parameter choice.


[1] J Liphardt, F Ritort, and C Bustamante. The nonequilibrium thermodynamics of small systems. *Phys. Today*, 58(7):43, 2005.

[2] Christopher Battle, Chase P Broedersz, Nikta Fakhri, Veikko F Geyer, Jonathon Howard, Christoph F Schmidt, and Fred C MacKintosh. Broken detailed balance at mesoscopic scales in active biological systems. *Science*, 352(6285):604–607, 2016.

[3] Daniel S Seara, Vikrant Yadav, Ian Linsmeier, A Pasha Tabatabai, Patrick W Oakes, SM Ali Tabei, Shiladitya Banerjee, and Michael P Murrell. Entropy production rate is maximized in non-contractile actomyosin. *Nature communications*, 9(1):1–10, 2018.

[4] Juan Pablo Gonzalez, John C. Neu, and Stephen W. Teitsworth. Experimental metrics for detection of detailed balance violation. *Phys. Rev. E*, 99:022143, Feb 2019.

[5] Takahiro Harada and Shin-ichi Sasa. Equality connecting energy dissipation with a violation of the fluctuation-response relation. *Physical review letters*, 95(13):130602, 2005.

[6] Boris Lander, Jakob Mehl, Valentin Blickle, Clemens Bechinger, and Udo Seifert. Noninvasive measurement of dissipation in colloidal systems. *Physical Review E*, 86(3):030401, 2012.

[7] S Muy, A Kundu, and D Lacoste. Non-invasive estimation of dissipation from non-equilibrium fluctuations in chemical reactions. *The Journal of chemical physics*, 139(12):09B645_1, 2013.

[8] JMR Parrondo and B Jiménez de Cisneros. Energetics of Brownian motors: a review. *Applied Physics A*, 75(2):179–191, 2002.

[9] Édgar Roldán and Juan MR Parrondo. Estimating dissipation from single stationary trajectories. *Physical review letters*, 105(15):150607, 2010.

[10] Junang Li, Jordan M Horowitz, Todd R Gingrich, and Nikta Fakhri. Quantifying dissipation using fluctuating currents. *Nature communications*, 10(1):1666, 2019.

[11] Federico S Gnesotto, Grzegorz Gradziuk, Pierre Ronceray, and Chase P Broedersz. Learning the non-equilibrium dynamics of brownian movies. *arXiv preprint arXiv:2001.08642*, 2020.

[12] Simon Tusch, Anupam Kundu, Gatien Verley, Thibaud Blondel, Vincent Miralles, Damien Démoulin, David Lacoste, and Jean Baudry. Energy versus information based estimations of dissipation using a pair of magnetic colloidal particles. *Physical Review Letters*, 112(18):180604, 2014.

[13] RKP Zia and B Schmittmann. Probability currents as principal characteristics in the statistical mechanics of non-equilibrium steady states. *Journal of Statistical Mechanics: Theory and Experiment*, 2007(07):P07012, 2007.

[14] Anna Frishman and Pierre Ronceray. Learning force fields from stochastic trajectories. *Physical Review X*, 10(2):021009, 2020.

[15] Hong Qian. Mesoscopic nonequilibrium thermodynamics of single macromolecules and dynamic entropy-energy compensation. *Physical Review E*, 65(1):016102, 2001.

[16] Christian Van den Broeck and Massimiliano Esposito. Three faces of the second law. ii. fokker-planck formulation. *Physical Review E*, 82(1):011144, 2010.

[17] Laura Pérez García, Jaime Donlucas Pérez, Giorgio Volpe, Alejandro V Arzola, and Giovanni Volpe. High-performance reconstruction of microscopic force fields from brownian trajectories. *Nature communications*, 9(1):1–9, 2018.

[18] Hervé Turlier, Dmitry A Fedosov, Basile Audoly, Thorsten Auth, Nir S Gov, Cécile Sykes, J-F Joanny, Gerhard Gompper, and Timo Betz. Equilibrium physics breakdown reveals the active nature of red blood cell flickering. *Nature physics*, 12(5):513–519, 2016.

[19] Kirsty Y Wan and Raymond E Goldstein. Time irreversibility and criticality in the motility of a flagellate microorganism. *Physical review letters*, 121(5):058103, 2018.

[20] Udo Seifert. Stochastic thermodynamics: principles and perspectives. *The European Physical Journal B*, 64(3):423–431, 2008.

[21] Christopher Jarzynski. Equalities and inequalities: Irreversibility and the second law of thermodynamics at the nanoscale. *Annu. Rev. Condens. Matter Phys.*, 2(1):329–351, 2011.

[22] Udo Seifert. Stochastic thermodynamics, fluctuation theorems and molecular machines. *Rep. Prog. Phys.*, 75(12):126001, 2012.

[23] Sreekanth K. Manikandan, Lennart Dabelow, Ralf Eichhorn, and Supriya Krishnamurthy. Efficiency fluctuations in microscopic machines. *Phys. Rev. Lett.*, 122:140601, Apr 2019.

[24] Ignacio A Martínez, Édgar Roldásupkrishnamurthyn, Luis Dinis, and Raúl A Rica. Colloidal heat engines: a review. *Soft matter*, 13(1):22–36, 2017.

[25] Gatien Verley, Massimiliano Esposito, Tim Willaert, and Christian Van den Broeck. The unlikely carnot efficiency. *Nat. Commun.*, 5:4721, 2014.

[26] Gatien Verley, Tim Willaert, Christian Van den Broeck, and Massimiliano Esposito. Universal theory of efficiency fluctuations. *Physical Review E*, 90(5):052145, 2014.

[27] Govind Paneru, Dong Yun Lee, Jong-Min Park, Jin Tae Park, Jae Dong Noh, and Hyuk Kyu Pak. Optimal tuning of a brownian information engine operating in a nonequilibrium steady state. *Physical Review E*, 98(5):052119, 2018.

[28] Juan MR Parrondo, Jordan M Horowitz, and Takahiro Sagawa. Thermodynamics of information. *Nature physics*, 11(2):131–139, 2015.

[29] Ignacio A Martínez, Gili Bisker, Jordan M Horowitz, and Juan MR Parrondo. Inferring broken detailed balance in the absence of observable currents. *Nature communications*, 10(1):1–10, 2019.

[30] Étienne Fodor, Wylie W Ahmed, Maria Almonacid, Matthias Bussonnier, Nir S Gov, M-H Verlhac, Timo Betz, Paolo Visco, and Frédéric van Wijland. Nonequilibrium dissipation in living oocytes. *EPL (Europhysics Letters)*, 116(3):30008, 2016.

[31] Shoichi Toyabe, Hong-Ren Jiang, Takenobu Nakamura, Yoshihiro Murayama, and Masaki Sano. Experimental test of a new equality: Measuring heat dissipation in an optically driven colloidal system. *Phys. Rev. E*, 75:011122, Jan 2007.

[32] Ken Sekimoto. Kinetic characterization of heat bath and the energetics of thermal ratchet models. *Journal of the physical society of Japan*, 66(5):1234–1237, 1997.

[33] Ken Sekimoto. Langevin equation and thermodynamics. *Progress of Theoretical Physics Supplement*, 130:17–27, 1998.

[34] U. Seifert. Entropy production along a stochastic trajectory and an integral fluctuation theorem. *Phys. Rev. Lett.*, 95:040602, 2005.

[35] Christian Maes and Karel Netočnỳ. Time-reversal and entropy. *Journal of statistical physics*, 110(1):269–310, 2003.

[36] Pierre Gaspard. Time-reversed dynamical entropy and irreversibility in markovian random processes. *Journal of statistical physics*, 117(3):599–615, 2004.

[37] David Andrieux, Pierre Gaspard, Sergio Ciliberto, N Garnier, Sylvain Joubaud, and Artyom Petrosyan. Thermodynamic time asymmetry in non-equilibrium fluctuations. *Journal of Statistical Mechanics: Theory*

*and Experiment*, 2008(01):P01002, 2008.

[38] D. Andrieux, P. Gaspard, S. Ciliberto, N. Garnier, S. Joubaud, and A. Petrosyan. Entropy production and time asymmetry in nonequilibrium fluctuations. *Phys. Rev. Lett.*, 98:150601, Apr 2007.

[39] Ryoichi Kawai, Juan MR Parrondo, and Christian Van den Broeck. Dissipation: The phase-space perspective. *Physical review letters*, 98(8):080602, 2007.

[40] R. A. Blythe. Reversibility, Heat Dissipation, and the Importance of the Thermal Environment in Stochastic Models of Nonequilibrium Steady States. *Physical Review Letters*, 100(1):010601, jan 2008.

[41] S. Vaikuntanathan and C. Jarzynski. Dissipation and lag in irreversible processes. *EPL (Europhysics Letters)*, 87(6):60005, sep 2009.

[42] S Muy, Anupam Kundu, and David Lacoste. Non-invasive estimation of dissipation from non-equilibrium fluctuations in chemical reactions. *The Journal of chemical physics*, 139:124109, 2013.

[43] Andre C. Barato and Udo Seifert. Thermodynamic uncertainty relation for biomolecular processes. *Phys. Rev. Lett.*, 114:158101, Apr 2015.

[44] Jordan M. Horowitz and Todd R. Gingrich. Proof of the finite-time thermodynamic ivcertainty relation for steady-state currents. *Phys. Rev. E*, 96:020103, Aug 2017.

[45] Todd R. Gingrich, Jordan M. Horowitz, Nikolay Perunov, and Jeremy L. England. Dissipation bounds all steady-state current fluctuations. *Phys. Rev. Lett.*, 116:120601, Mar 2016.

[46] Udo Seifert. From stochastic thermodynamics to thermodynamic inference. *Annual Review of Condensed Matter Physics*, 10(1):171–192, 2019.

[47] Jordan M Horowitz and Todd R Gingrich. Thermodynamic uncertainty relations constrain non-equilibrium fluctuations. *Nature Physics*, 16(1):15–20, 2020.

[48] Sreekanth K Manikandan, Deepak Gupta, and Supriya Krishnamurthy. Inferring entropy production from short experiments. *arXiv preprint arXiv:1910.00476*, 2019.

[49] Shun Otsubo, Sosuke Ito, Andreas Dechant, and Takahiro Sagawa. Estimating entropy production by machine learning of short-time fluctuating currents. *Physical Review E*, 101(6):062106, 2020.

[50] Tan Van Vu, Van Tuan Vo, and Yoshihiko Hasegawa. Entropy production estimation with optimal current. *arXiv preprint arXiv:2001.07131*, 2020.

[51] Dong-Kyum Kim, Youngkyoung Bae, Sangyun Lee, and Hawoong Jeong. Learning entropy production via neural networks. *Phys. Rev. Lett.*, 125:140604, Oct 2020.

[52] Lukas P Fischer, Hyun-Myung Chun, and Udo Seifert. Free diffusion bounds the precision of currents in underdamped dynamics. *Physical Review E*, 102(1):012120, 2020.

[53] Sanjib Sabhapandit. Work fluctuations for a harmonic oscillator driven by an external random force. *EPL (Europhysics Letters)*, 96(2):20005, 2011.

[54] Gatien Verley, Christian Van den Broeck, and Massimiliano Esposito. Work statistics in stochastically driven systems. *New Journal of Physics*, 16(9):095001, 2014.

[55] Sreekanth K. Manikandan and Supriya Krishnamurthy. Asymptotics of work distributions in a stochastically driven system. *The European Physical Journal B*, 90(12):258, Dec 2017.

[56] Sreekanth K Manikandan and Supriya Krishnamurthy. Exact results for the finite time thermodynamic uncertainty relation. *J. Phys. A: Math. Theor.*, 51(11):11LT01, 2018.

[57] Juan Ruben Gomez-Solano, Ludovic Bellon, Artyom Petrosyan, and Sergio Ciliberto. Steady-state fluctuation relations for systems driven by an external random force. *EPL (Europhysics Letters)*, 89(6):60003, 2010.

[58] E Dieterich, J Camunas-Soler, M Ribezzi-Crivellari, U Seifert, and F Ritort. Single-molecule measurement of the effective temperature in non-equilibrium steady states. *Nature Physics*, 11(11):971–977, 2015.

[59] Arnab Pal and Sanjib Sabhapandit. Work fluctuations for a brownian particle in a harmonic trap with fluctuating locations. *Phys. Rev. E*, 87:022138, Feb 2013.

[60] Yudong Zhang, Shuihua Wang, and Genlin Ji. A comprehensive survey on particle swarm optimization algorithm and its applications. *Mathematical Problems in Engineering*, 2015, 2015.

[61] Maurice Clerc. Confinements and biases in particle swarm optimisation. 2006.

[62] Thomas Speck, Jakob Mehl, and Udo Seifert. Role of external flow and frame invariance in stochastic thermodynamics. *Phys. Rev. Lett.*, 100:178302, Apr 2008.

[63] Tan Van Vu and Yoshihiko Hasegawa. Uncertainty relations for underdamped langevin dynamics. *Phys. Rev. E*, 100:032130, Sep 2019.

[64] Jae Sung Lee, Jong-Min Park, and Hyunggyu Park. Thermodynamic uncertainty relation for underdamped langevin systems driven by a velocity-dependent force. *Phys. Rev. E*, 100:062132, Dec 2019.

[65] Oliver Niggemann and Udo Seifert. Field-theoretic thermodynamic uncertainty relation. *Journal of Statistical Physics*, 178(5):1142–1174, 2020.

[66] Sebastian Hurst, Bart E Vos, and Timo Betz. Intracellular softening and fluidification reveals a mechanical switch of cytoskeletal material contributions during division. *bioRxiv*, pages 2021–01, 2021.

[67] Shun Otsubo, Sreekanth K Manikandan, Takahiro Sagawa, and Supriya Krishnamurthy. Estimating entropy production along a single non-equilibrium trajectory. *arXiv preprint arXiv:2010.03852*, 2020.

[68] Sudipta Bera, Shuvojit Paul, Rajesh Singh, Dipanjan Ghosh, Avijit Kundu, Ayan Banerjee, and R Adhikari. Fast bayesian inference of optical trap stiffness and particle diffusion. *Scientific reports*, 7(1):1–10, 2017.

[69] Subhrokoli Ghosh, Rajesh Singh, and Ayan Banerjee. Assembly and manipulation of mesoscopic particles using micro bubbles in thermo-optical tweezers. In *Optical Trapping and Optical Micromanipulation XV*, volume 10723, page 107232Q. International Society for Optics and Photonics, 2018.

[70] Subhrokoli Ghosh, Anand Dev Ranjan, Santu Das, Rakesh Sen, Basudev Roy, Soumyajit Roy, and Ayan Banerjee. Directed self-assembly driven mesoscale lithography using laser-induced and manipulated microbubbles: Complex architectures and diverse applications. *Nano Letters*, 21(1):10–25, 2021. PMID: 33296219.

**Supplemental Information**

**The heat dissipated in the medium for the case with the bubble**

In this work, we have obtained an estimate for the average total entropy production of a colloidal particle maintained in a steady state by being confined in a shaken trap (the stochastic sliding parabola model), under two different experimental conditions, namely without and with a microscopic bubble in the vicinity of the trap. The average total entropy production for a system in steady state is also the same as the heat dissipated by the system into the surrounding bath (at constant temperature $T$). This heat dissipated includes the heat associated with keeping the system in a steady state (by shaking the trap) and, if there is a flow, the heat associated with the work done by the flow on the particle. As we argue below, the latter component cannot be obtained by the short-time inference scheme, and is related to a fundamental limitation of the applicability of the TUR [46] related to how the flow term is dealt with.

We begin with a possible generic form of the Langevin equation in the presence of the bubble,

$$\dot{x} - u_d = -\frac{(x-\lambda)}{\tau_d} + \sqrt{2D_d}\,\eta(t), \tag{22}$$

$$\dot{\lambda} = -\frac{\lambda}{\tau_0} + \sqrt{2A}\,\xi(t), \tag{23}$$

where $u$, $\tau$ and $D$ are taken to be slowly varying functions of $x$, and essentially treated as constants ($u_d$, $\tau_d$ and $D_d$) at a distance $d$ from the bubble, where the particle is trapped.

First, we notice that under the transformations $x \to x' = x - \tau_d u_d$, the above equations map to the Stochastic sliding parabola model, with the parameters $\tau = \tau_d$ and $D = D_d$. This observation also demonstrates that for the above system, the mean position of the particle is no longer at the center of the trap, but is instead $\langle x \rangle = u_d \tau_d$. Now we look at the entropy production in this system, using the standard definitions in Stochastic thermodynamics.

Since the system is in a stationary state, the actual rate of entropy production can be obtained in terms of the heat ($q$) dissipated to the medium at a temperature $T$ as,

$$\sigma = \frac{q}{T}. \tag{24}$$

However there is an ambiguity on how to obtain the correct value of $\sigma$, arising from two choices of transformations for the flow term under time-reversal [62].

The first approach is to let the flow term reverse it's sign under time-reversal, as physically meaningful for a velocity variable. This gives an estimate of medium entropy production [62] as,

$$\begin{aligned} \sigma &= \frac{q}{T} \\ &= \frac{\langle (\dot{x} - u_d)(-\nabla_x V) \rangle}{T} \\ &= \frac{\langle (\dot{x} - u_d)(\lambda - x) \rangle}{T}. \end{aligned} \tag{25}$$

The observed trajectories of the colloidal particle, on the other hand, only show the effect of the flow $u_d$ as a constant external force acting on the system, which only amounts to shifting the mean position of the colloidal particle in the direction of the flow. This leads to a second (naive) approach to the entropy production in this system as,

$$\begin{aligned} \sigma' &= \frac{\langle \dot{x}(-\nabla_x V + u_d \tau_d) \rangle}{T} \\ &= \frac{\langle \dot{x}(\lambda - x + u_d \tau_d) \rangle}{T}. \end{aligned} \tag{26}$$

The physical distinction between the two definitions is as follows: when there is a background flow in the medium, this flow has to constantly do work against the confining potential to maintain the particle in it's "new" average position.This is an additional contribution to entropy production, that is only accounted for in the definition in Eq. (25). In other words, the particle trajectories do not carry information about this and hence the short-time inference

scheme, which is based on TUR and the information carried by particle trajectories, only predicts the quantity $\sigma'$ in Eq. (26). $\sigma$ and $\sigma'$ are related by,

$$\begin{aligned}\sigma &= \sigma' + \frac{u_d^2 \tau_d}{T}, \\ &\geq \sigma'.\end{aligned} \tag{27}$$

When the flow velocity $u_d = 0$, they are the same.

### Currents in the non-equilibrium stationary state

Systems in a non-equilibrium stationary state are characterized by a non-vanishing current in the phase space [2]. For the colloidal system we consider, these currents can be estimated from the trajectory data as,

$$\begin{bmatrix} J_x(x,\lambda) \\ J_\lambda(x,\lambda) \end{bmatrix} = \left[ \left\langle \begin{matrix} x(t+\Delta t) - x(t) \\ \lambda(t+\Delta t) - \lambda(t) \end{matrix} \right\rangle_{x,\lambda} \right. \tag{28}$$

$$\left. - \left\langle \begin{matrix} x(t) - x(t-\Delta t) \\ \lambda(t) - \lambda(t-\Delta t) \end{matrix} \right\rangle_{x,\lambda} \right] \frac{P_{ss}(x,\lambda)}{2\Delta t}. \tag{29}$$

For the case without the bubble, this estimate converges to the expressions in Eq. (10b) if we have sufficient amount of data. In Figure. 8, we demonstrate this for certain parameter choices in Fig. 2.

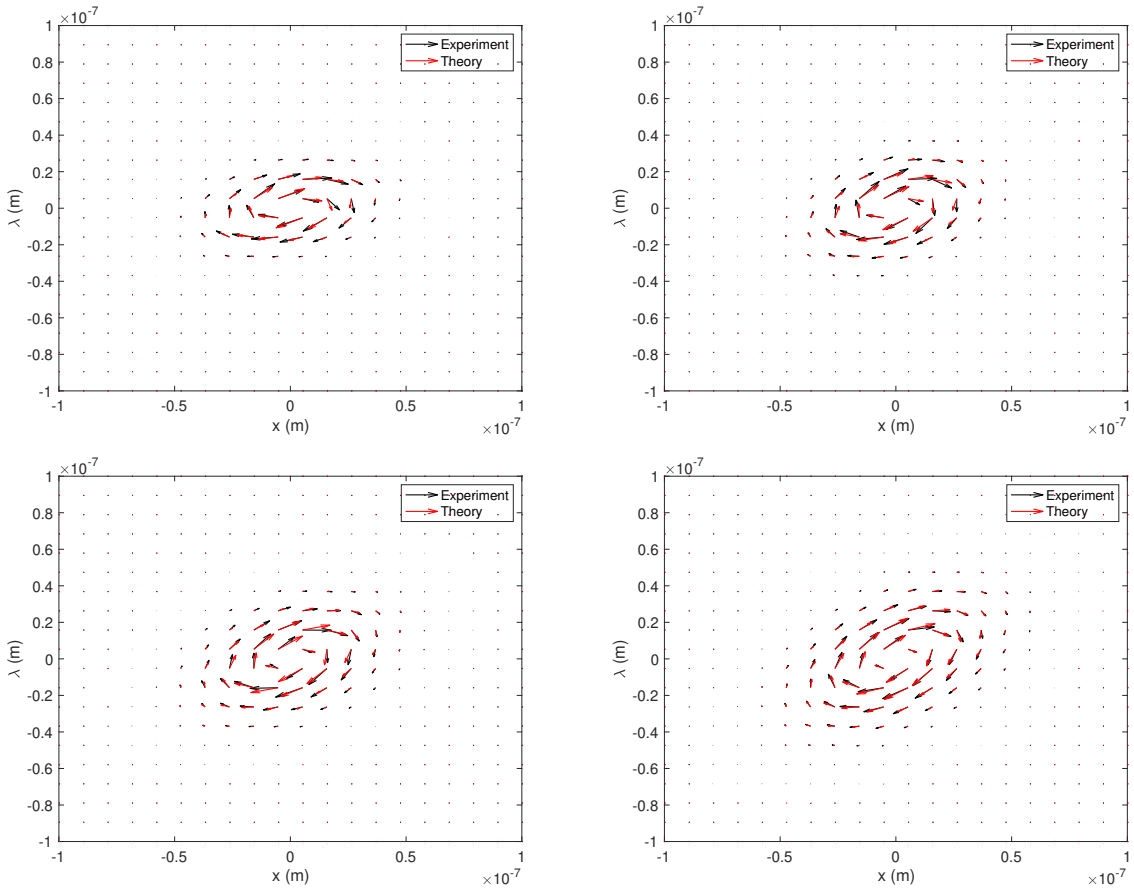


FIG. 8. Steady state currents obtained from experimental data (Eq. (28)) compared to theory (Eq. (10b)) for certain parameters in Fig. 2. The parameters correspond to $A = [0.1,\ 0.15,\ 0.3,\ 0.2] \times (0.6 \times 10^{-6})^2 m^2 s^{-1}$ in clockwise order.

.

Using Eq. (28) we further estimate currents in the case when the bubble is present in the vicinity of the optical trap. We find that the phase space currents are reduced in magnitude. We demonstrate this with surface plots of the two components of the currents in Fig. 9 for the case discussed in Figure 4 in the main text.

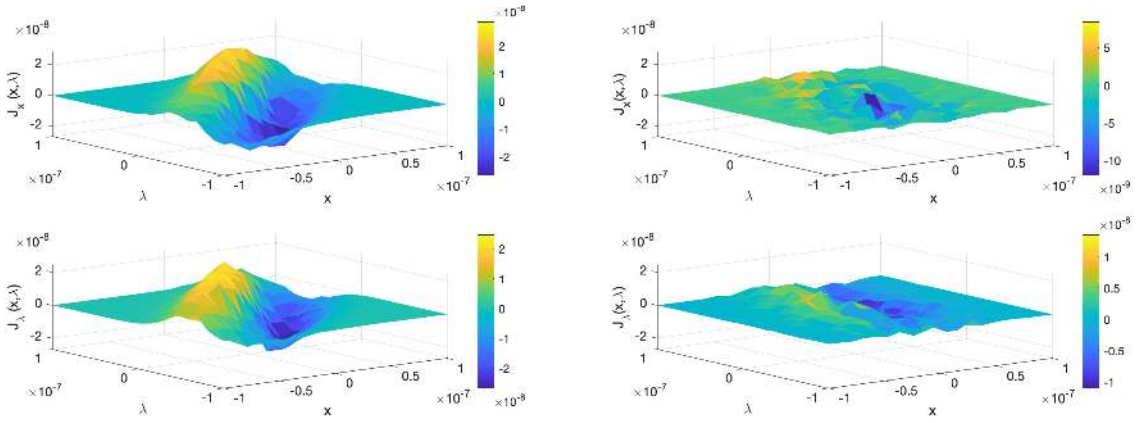

FIG. 9. Surface plots of the two components of the currents ($J_x$ and $J_\lambda$) (Eq. (28)) for the case discussed in Figure 4 of the main text. *Left:* Case without the bubble in the vicinity of the optical trap. *RIght:* Case with the bubble in the vicinity of the optical trap. We find that the magnitude of the currents are reduced in the vicinity of the bubble.

**Parameter values**

*Figure 1:* $\tau = \frac{1}{2\pi f_c} = 0.0012$, $\tau_0 = 0.0025$, $D = 1.6452\times10^{-13}$, $A = [0.1,\ 0.15,\ 0.2,\ 0.25,\ 0.3,\ 0.35]\times(0.6\times10^{-6})^2$.

*Figure 2:* $f_c = 135 \pm 10$, $\tau_0 = 0.0025$, $D = 1.6452 \times 10^{-13}$, $A = [0.1,\ 0.15,\ 0.2,\ 0.25,\ 0.3,\ 0.35] \times (0.6 \times 10^{-6})^2$. The shaded light-blue region accounts for a $\pm10$ error bar from the $f_c$ fluctuations in the experiment.

*Figure 4:* $f_c = 57 \pm 3\ Hz$, $\tau_0 = 0.025$, $D = 1.6452 \times 10^{-13}$, $A = 0.3 \times (0.6 \times 10^{-6})^2$.

*Figure 5:* $f_c = 135 \pm 10\ Hz$, $\tau_0 = 0.0025$, $D = 1.6452 \times 10^{-13}$, $A = 0.3 \times (0.6 \times 10^{-6})^2$.

# Figures

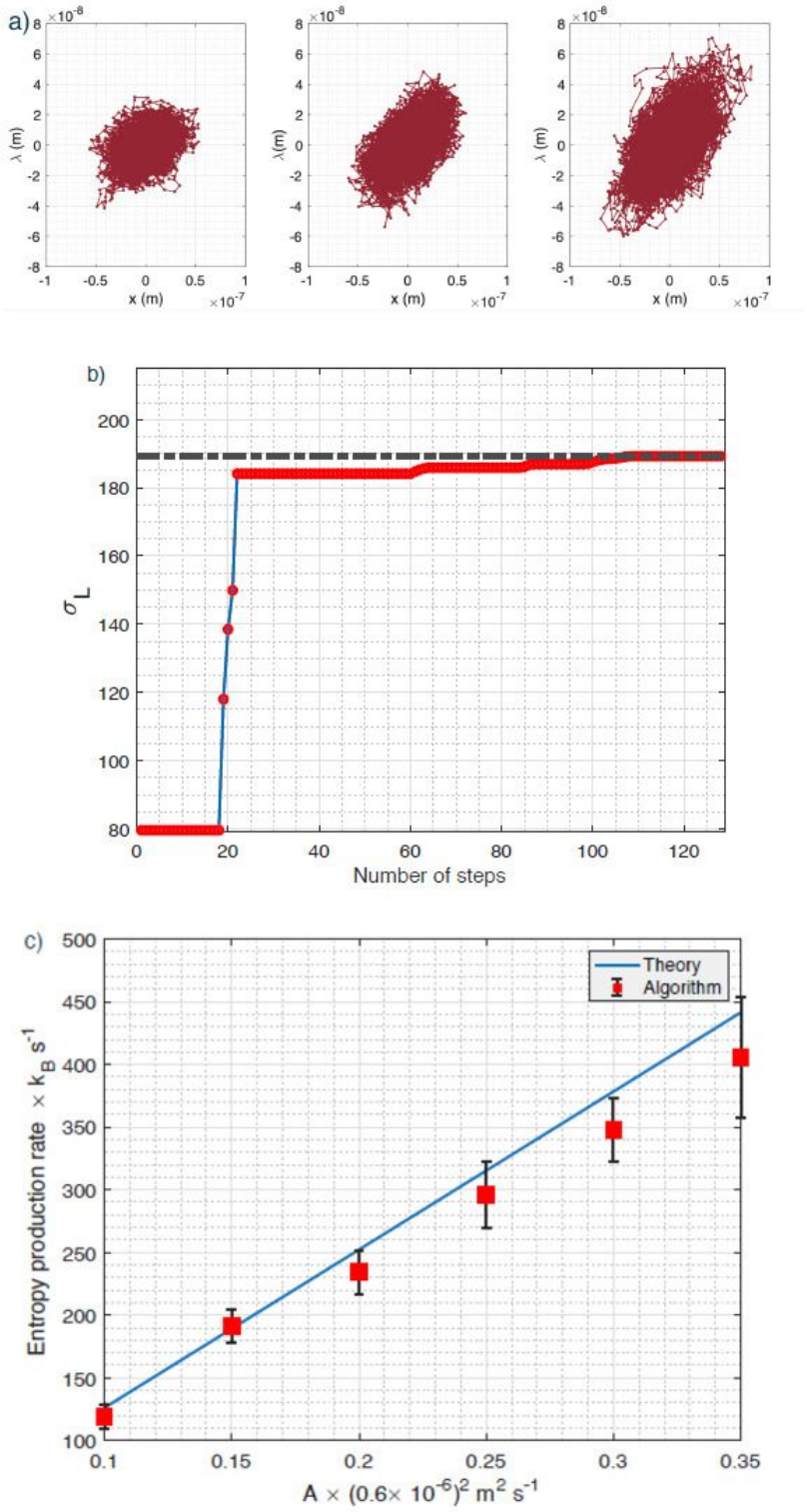


**Figure 1**

The inference algorithm tested on numerically gener- ated data. a) Brownian trajectories of the Stochastic sliding parabola for A = 0:1, 0:25 and 0:35. b) The inferred entropy production rate plotted against the

number of steps in the op- timization process for A = 0:15 with Δt = 0:0001. c) Inferred entropy production as a function of the parameter A.

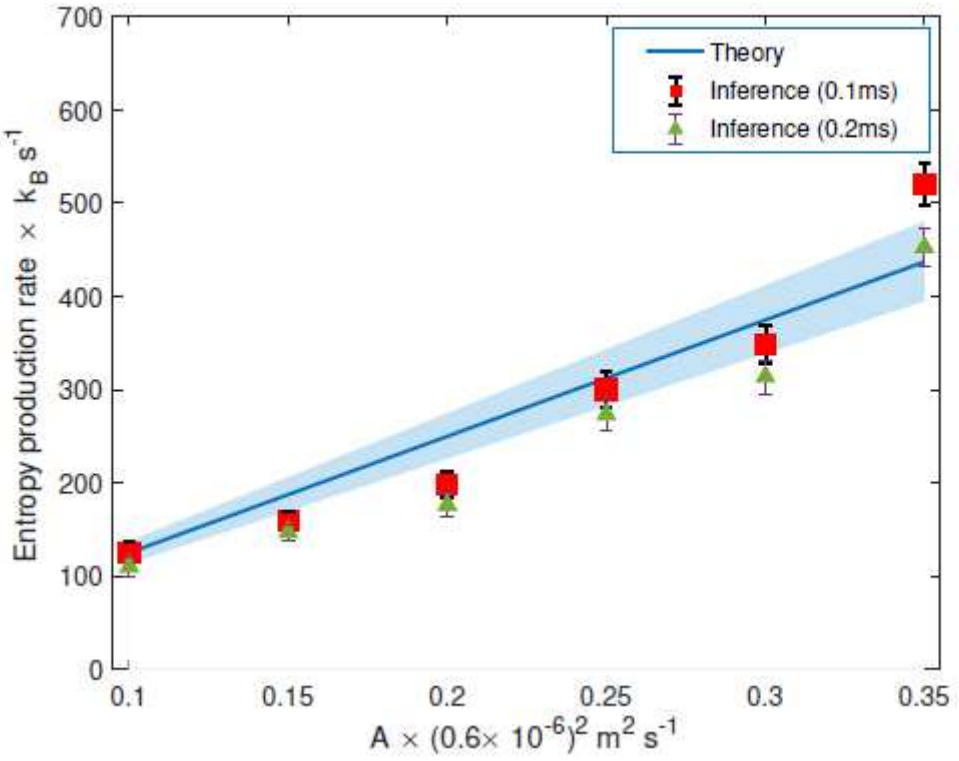


**Figure 2**

Inference algorithm tested on the experimental data for different values of the parameter A. The blue line corre- sponds to the theoretical value, and the squares corresponds to σ estimated from the experimental data. The shaded blue region accounts for fc uctuations theoretically (see the sup- plemental information).

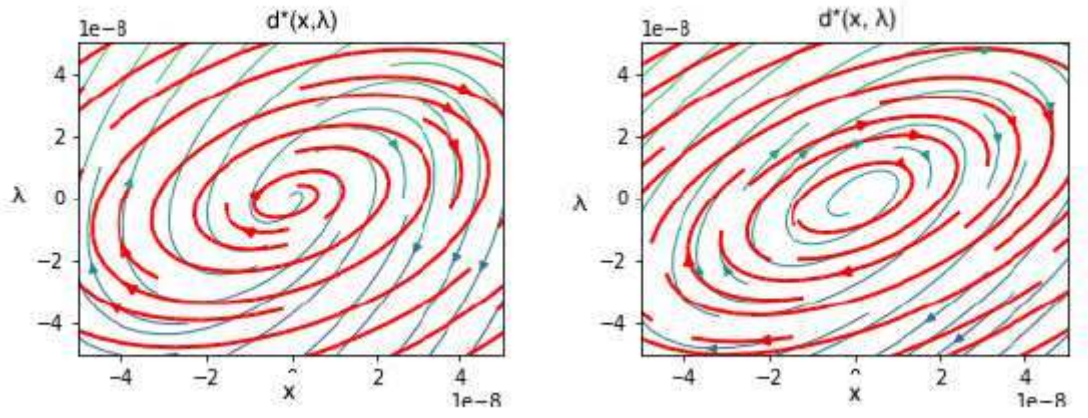


**Figure 3**

See manuscript for full figure caption.

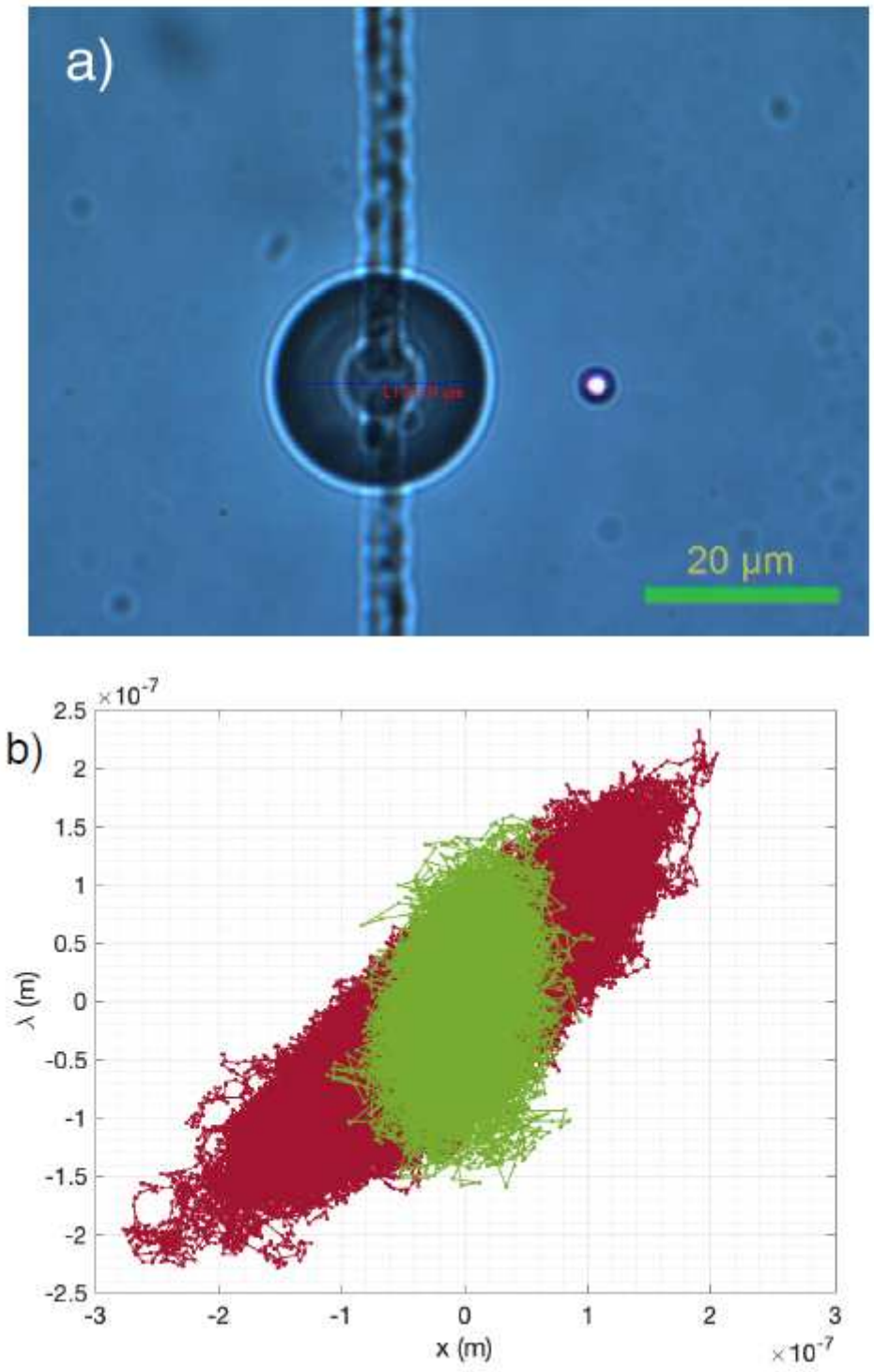


**Figure 4**

The colloidal system in the presence of the bubble. a) The microbubble - colloidal particle system. b) System trajectories without (red) and with (green) the bubble in the neighbourhood of the colloidal particle. We see that the colloidal particle is strongly conned in the presence of the bubble.

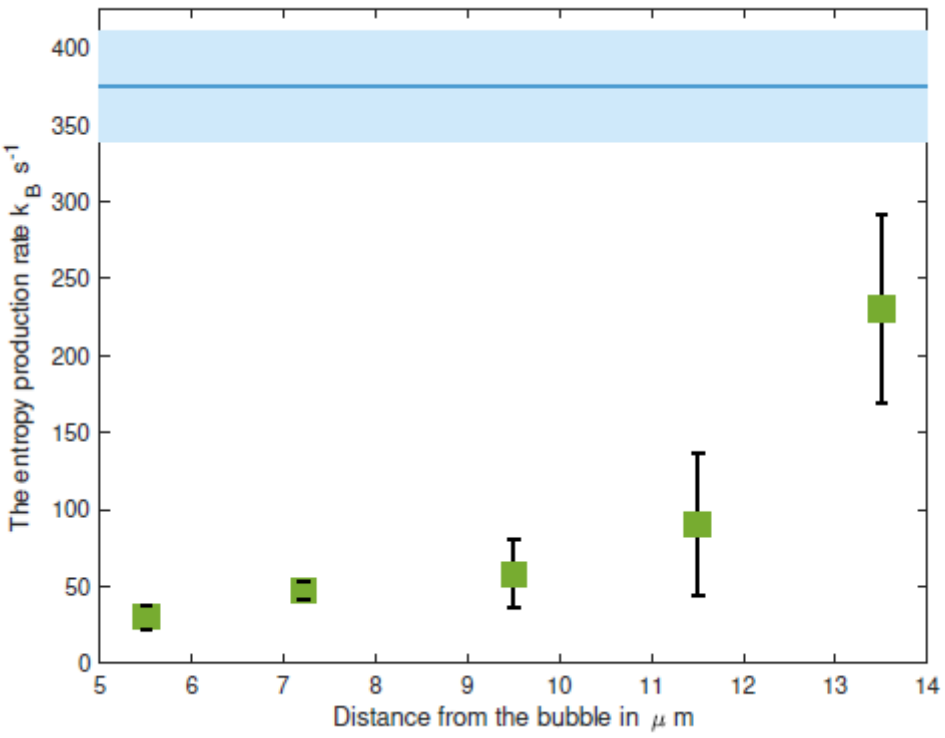


**Figure 5**

TUR estimate of entropy production in the colloidal system in the presence of the bubble, as a function of the distance from the surface of the bubble.

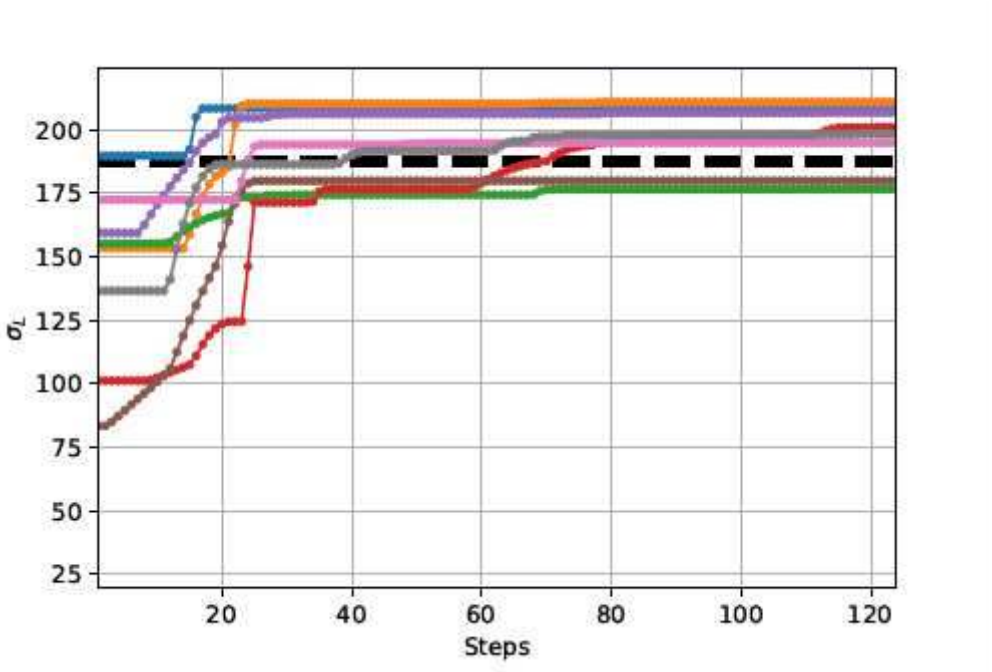


**Figure 6**

The value of sigma inferred (σL) as a function of the number of steps in the optimization algorithm for different 12.5s data sets, that are numerically generated for the same parameter choice as in Figure 1b of the main text. The black dashed-line corresponds to the theoretical estimate of σ for this parameter choice.

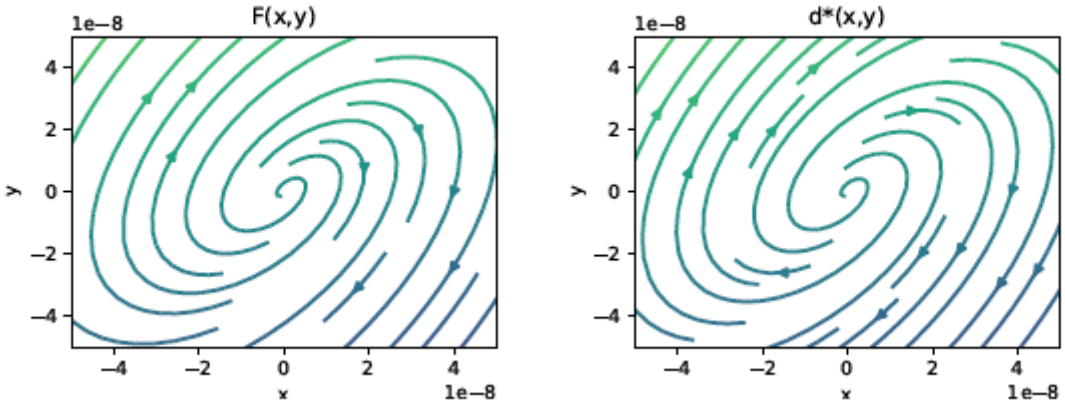


**Figure 7**

See manuscript for full figure caption.

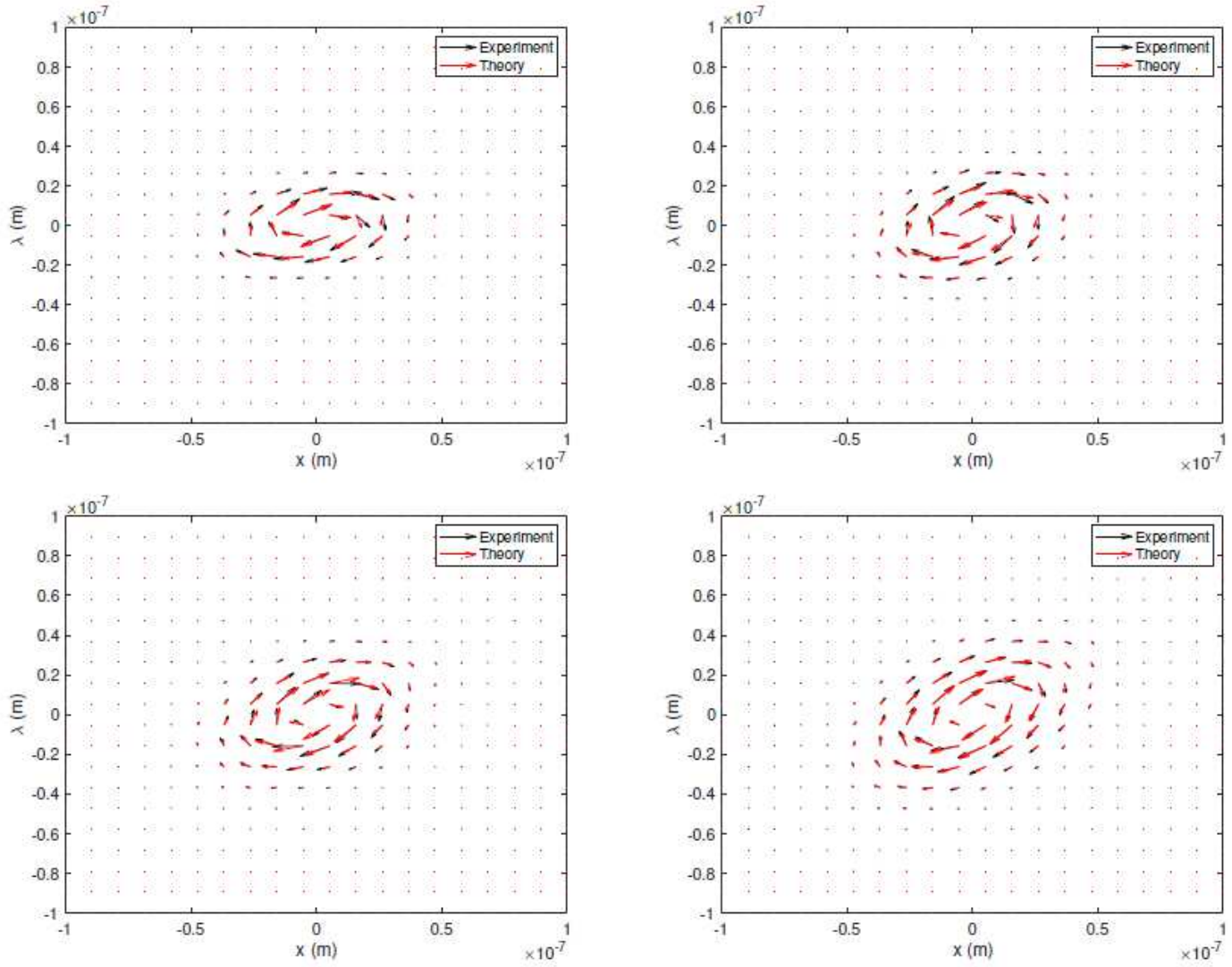


## Figure 8

See manuscript for full figure caption.

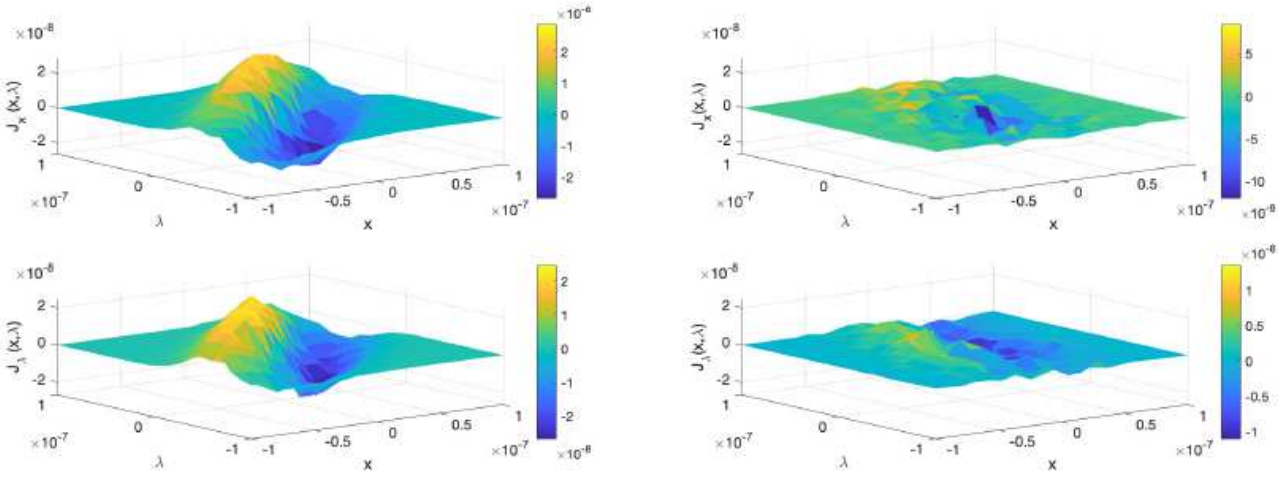

## Figure 9

Surface plots of the two components of the currents (Jx and Jλ) (Eq. (28)) for the case discussed in Figure 4 of the main text. Left: Case without the bubble in the vicinity of the optical trap. Right: Case with the bubble in the vicinity of the optical trap. We nd that the magnitude of the currents are reduced in the vicinity of the bubble.